Melt Pool Characterization for Selective Laser Melting of Ti-6Al-4V Pre-alloyed Powder

Haijun Gong, Hengfeng Gu, Kai Zeng, J.J.S. Dilip, Deepankar Pal, Brent Stucker
Department of Industrial Engineering
J. B. Speed School of Engineering, University of Louisville, Louisville, KY 40292

Daniel Christiansen, Jack Beuth
Department of Mechanical Engineering
College of Engineering, Carnegie Mellon University, Pittsburgh, PA 15213

John J. Lewandowski
Department of Materials Science & Engineering
Case School of Engineering, Case Western Reserve University, Cleveland, OH 44106

`REVIEWED`

Abstract

Parameter optimization for metal powders in Selective Laser Melting (SLM) is usually carried out by experimental investigations of the influence of significant parameters (such as laser power, scan speed, hatch spacing, layer thickness, scan pattern, etc.) on microstructure and/or mechanical properties. This type of experimental optimization is extremely time- and cost-consuming. In order to accelerate the optimization process, a study was undertaken to develop a method for rapid optimization of parameters based on melt pool characterizations. These characterizations began with investigations of SLM single bead experiments. Pre-alloyed Ti-6Al-4V powder was used for single bead fabrication with multiple laser power and scan speed combinations. Surface morphology and dimensions of single beads were characterized. Geometrical features of melt pools were measured after polishing and etching of the cross section of each single bead. It was found that melt pool characteristics provide significant information that is helpful for process parameters selection. These experiments are being extended to characterize test pads with multiple layers.

Introduction

Selective Laser Melting (SLM) is one of the most popular powder bed fusion based Additive Manufacturing (AM) processes [1]. This technology was successfully demonstrated early this century and then commercialized by several companies, such as EOS GmbH, Concept Laser GmbH, SLM Solutions GmbH, Realizer GmbH, Phenix System, MTT Technologies, etc. The latter two were acquired by 3D Systems in 2013, and by Renishaw in 2011 respectively. Currently, increasing the capability of commercialized SLM machines has focused on improving build dimensions, speed, and material compatibility. EOS, Concept Laser, and SLM Solutions have introduced SLM machines containing large build platforms, such as the EOS M400, Concept Laser X-line 1000R (*X*-axis up to 630 millimeters), and SLM® 500HL. By increasing layer thickness and recoating speed, the time to build a part can be greatly reduced. Increasing types of metallic powders can be utilized for SLM, including stainless steels, tool steels, and bio-compatible alloys.

The ability to quickly produce parts with multiple metallic powders has resulted in the applications of SLM to direct-part fabrication for aerospace, tooling, biomedical and other

256

technologies. However, process parameter optimization for new powders is very slow since it is usually carried out experimentally to determine a specific value of the influential parameters, such as laser power, scan speed, hatch spacing, layer thickness, scan pattern, etc. Samples created using selected parameter combinations are validated through density, porosity, microstructure and/or mechanical properties tests. This type of experimental optimization is extremely time- and cost-consuming. In order to accelerate the optimization process, this study was undertaken to develop a method for rapid optimization of parameters based on melt pool characterizations. Pre-alloyed Ti-6Al-4V powder was used to generate melt pool geometries by various laser power and scan speed combinations. The profile and dimensions of the melt pools were then evaluated and measured to select appropriate hatch spacing distance for fabricating test pads. Surface topology of pads was analyzed and discussed to select optimal parameters.

Method

The rapid optimization method for process parameters began with an investigation of SLM single bead experiments. EOS pre-alloyed Ti-6Al-4V powder was used for single bead fabrication with multiple laser power and scan speed combinations. The powder has an apparent density of 2.63 g/cm^3. Fig. 1 shows the powder morphology under a Scanning Electron Microscope (SEM). Most particles have a spherical or near-spherical morphology with small satellite particles attached. A small amount of solidified agglomerates of molten particles can also be observed. Based on a measurement using a Microtrac S3000 laser-based particle size analyzer, the powder particles show a size distribution between 25 μm (D_{10}) and 53 μm (D_{90}) with Mean Volume Diameter around 38 μm. The particle size is nearly normally distributed.
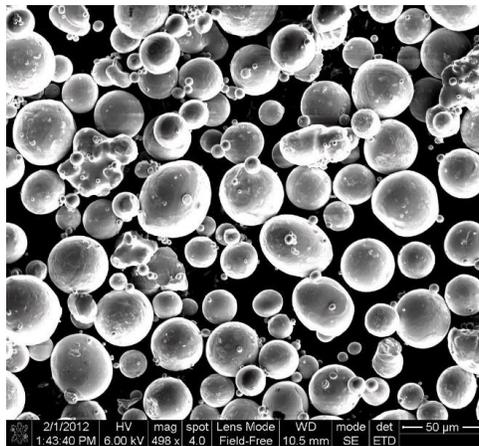
Fig. 1 SEM of EOS Ti-6Al-4V powder morphology

An EOS M270 Direct Metal Laser Sintering (DMLS) system was utilized in this study. The system uses an Yb-fiber laser with nominal maximum power 200W. A focused laser beam is guided and positioned through an optical system to the desired sites of the powder bed to melt metallic powder. In order to characterize the dimensions and surface topology of the melt pools, a factorial design of experiment (DOE) was performed with multiple combinations of laser power and scan speed. The experimental factors and levels are given in Table 1. Base plate was preheated to 35 °C. Single scans were conducted to form single beads on a bare base plate (no powder case) and a base plate with one layer of Ti-6Al-4V powder (powder case, 30 μm), respectively but using the same parameter combinations. Therefore, there are 42 single beads for each case.

Table 1 Factors and Levels of Factorial DOE for Single Beads

Factor	Level
Laser Power (W)	50, 75, 100, 125, 150, 175, 195
Scan Speed (mm/s)	200, 400, 600, 800, 1000, 1200

Typically an EOS M270 DMLS system only allows Ti-6Al-4V powders to be melted at a layer thickness of 30 μm, therefore layer thickness was not considered a variable in this study. After evaluating the surface topology, all the single beads were sectioned, polished, and etched for measuring geometrical features of melt pools following standard metallography procedures. Hatch spacing distance for subsequent multi-layer pad studies was determined from the melt pool width of each single bead. Multi-layer pads (~1 mm in thickness) were then fabricated using selected parameter combinations using an alternating raster scan of each layer along the *X*-axis and *Y*-axis direction every other layer.

Results and Discussion

Surface topology of single beads

When a laser scan is performed on a bare base plate (no powder case), single beads are formed due to remelting and solidification of the plate material. All single beads were consistent without any interruption. The width variation of each single bead was not significant, except at the starting and ending sites which are larger due to speed ramping of the laser galvanometers. Fig. 2 shows a typical single bead which was generated along the *X*-axis using a laser power of 125W and scan speed of 200mm/s. It is noted that the melt pool shows a rounded front and prominent tail along the direction of motion. Melt pool geometry on the base plate could be easily reconstructed by observing the scan track.

Fig. 2 A typical single bead for a no powder case (125W & 200mm/s)

For some single beads, especially when created using low energy density, the melt pool geometry is hard to recognize. A small amount of material (or none at all) will be melted at low energy densities. Fig. 3 summarizes the high and low energy density situations, which indicate dissimilar surface topology for single beads on the base plate.
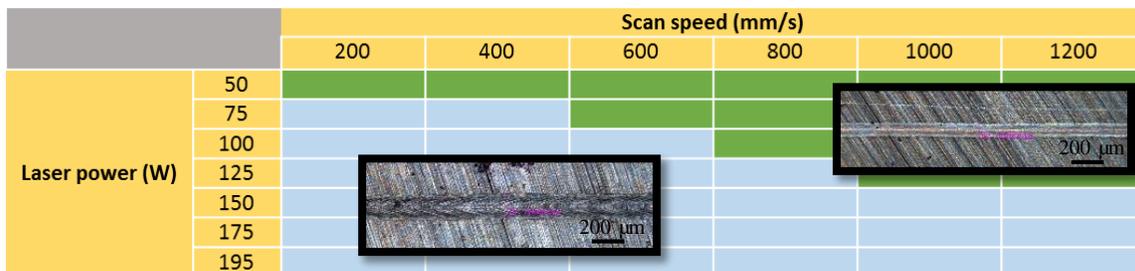
Fig. 3 Surface topology of single beads on the base plate (no powder case) where light blue denotes easy to identify melt pool geometries and green indicates little or no melt pool formation

For the powder case, the base plate was lowered 30 μm from the laser focal plane. One layer of Ti-6Al-4V powder was then spread by the recoating blade all over the base plate. It is hard to guarantee that the base plate is completely flat and perfectly leveled. So the layer thickness of powder may have varied slightly above or below 30 μm. Single beads were generated by melting powder and base plate material, which formed a uniform melt pool and solidified together. The single beads show similar melt pool geometry compared to the no powder case. But the surface roughness is worse because particles are attached to both sides of the single beads. Fig. 4 shows a single bead which was generated using the same parameters as Fig. 3 for the no powder case. It can be seen that speed ramping also causes larger starting and ending sites. But, compared to the no powder case, width variation is very significant, especially for parameter combinations with low energy density. Evidence for this is provided in subsequent sections.
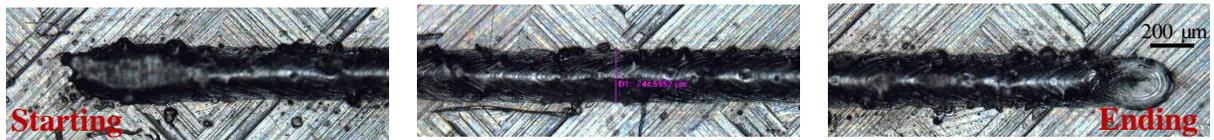
Fig. 4 A typical single bead of powder case (125W & 200mm/s)

The powder case is more complicated than the no powder case. In addition to the powder particles attached to the single beads, many holes can be observed on the top surface. These holes may be attributed to gas bubble ejection from the melt pool. When a laser spot with high energy density is applied to a powder bed, gas bubbles may form in the melt pool due to vaporization of low melting point constituents within the alloy [2]. The surface topology of single beads is shown in Fig. 5. It can be inferred that the vaporization phenomenon is important for the high energy density zone (red zone). If appropriate laser energy is used on the powder bed, a uniform single bead width can be expected. With appropriate process conditions, only a few holes appear for many single bead tracks (blue zone). But if laser energy is insufficient, single beads become interrupted and inconsistent due to lack of fusion (purple zone).
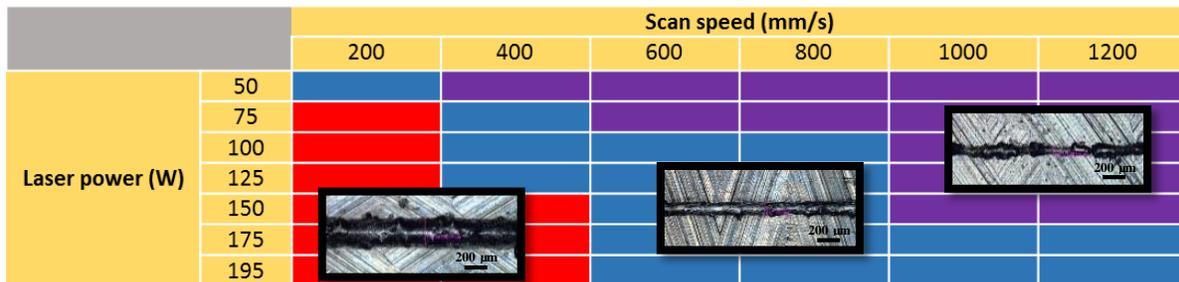
Fig. 5 Surface topology of single beads on the base plate (powder case) showing vaporization induced porosity (red zone) good melt pool characteristics (blue zone) and unstable melt pools (purple zone)

Each single bead was measured at multiple locations (far away from the starting and ending sites) for average width dimension. The average single bead width is illustrated in Fig. 6. Based on these measurements, single beads of powder show a slightly wider dimension compared to the no powder case, except for a few parameter combinations. This may be attributed to the lower thermal conductivity of the powder bed compared to a solid base plate and/or the enhanced laser

absorptivity of powders compared to solid materials. Due to the low thermal conductivity of metallic powder, a few amount of thermal energy, which is only conducted downward to the base plate, is accumulated in the powder bed resulting in a little wider dimension of single beads, compared to the no powder case. Otherwise, the largest single bead width always takes place at 195W & 200mm/s. Low laser power and/or fast scan speed usually result in a narrow single bead.
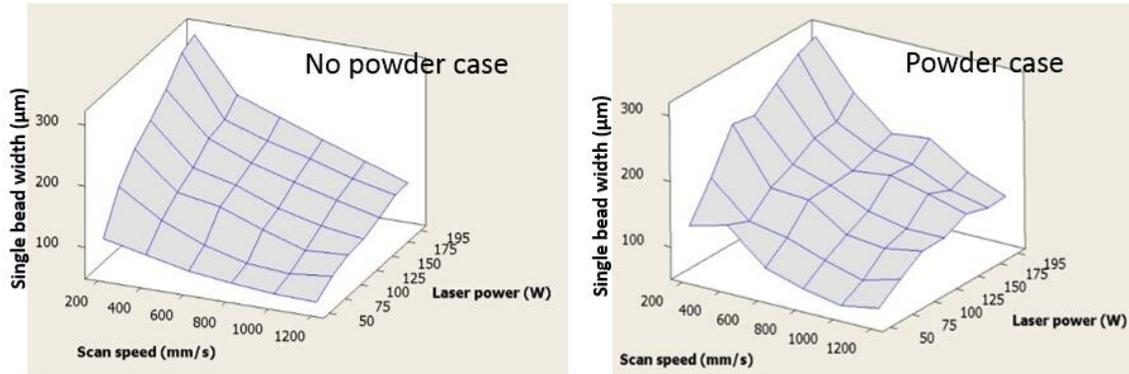
Fig. 6 3D visualization of average single bead width

Melt pool profiles of single beads

The surface topology of single beads provides valuable information about melt pool morphology and continuity of scan tracks. In order to further investigate melt pool morphology, all single beads were sectioned in the middle, perpendicularly to the scanning direction. Cross sections were then polished and etched for metallography to show dimensional and geometrical features. Fig. 7 shows cross sections of single beads (no powder case) fabricated using multiple laser power and scan speed combinations.

It can be seen that the melt pool profile is clearly distinguished from the base plate material. This is because the microstructure of the melt pool is transformed to α' phase (martensite) due to the fast cooling rate [3]. A heat affected zone can also be observed in the peripheral area of the melt pool. High laser power and/or low scan speed result in large melt pools. It is noted that pores are commonly included inside melt pools which have keyhole geometry for high energy density input. This may be attributed to gas bubbles entrapped in the melt pool due to material evaporation [4, 5].

Other than pores in the melt pool, there are two melt pools showing unusual profiles for a laser power of 195W and scan speeds of 400mm/s and 600mm/s. This may be caused by occasional laser power fluctuation during the melting process, since laser power instability is more likely at process extremes (195W is the maximum power for this laser) and thus fluctuations could cause lower amounts of energy and thus smaller melt pools, as shown in Fig. 8. Another possible theory is that melt pool fluid dynamics at higher energy densities could cause instabilities. The samples were happened to be sectioned around those locations, which show inconsistent melt pool profiles.
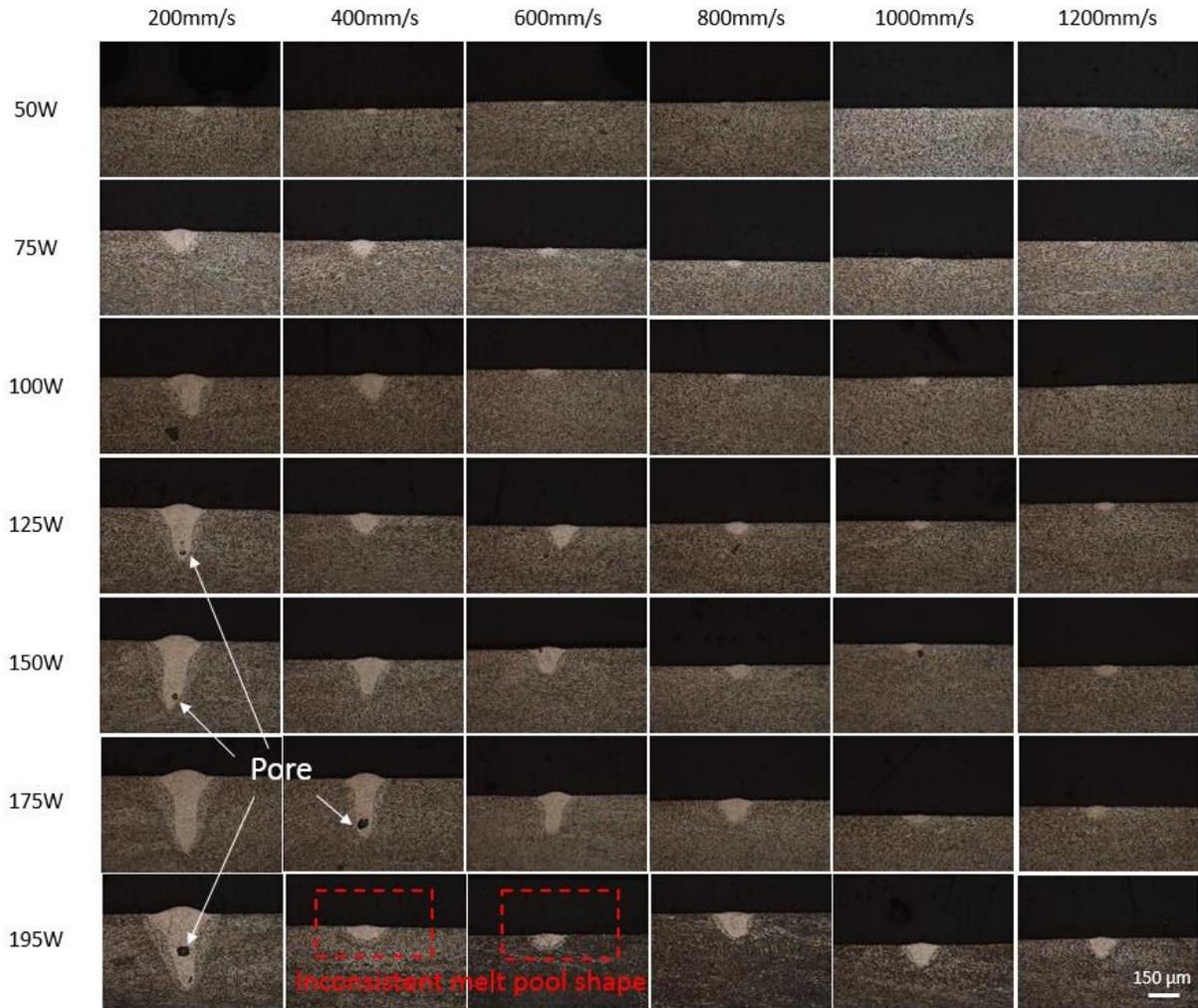
Fig. 7 Melt pool profile for single beads (no powder case)
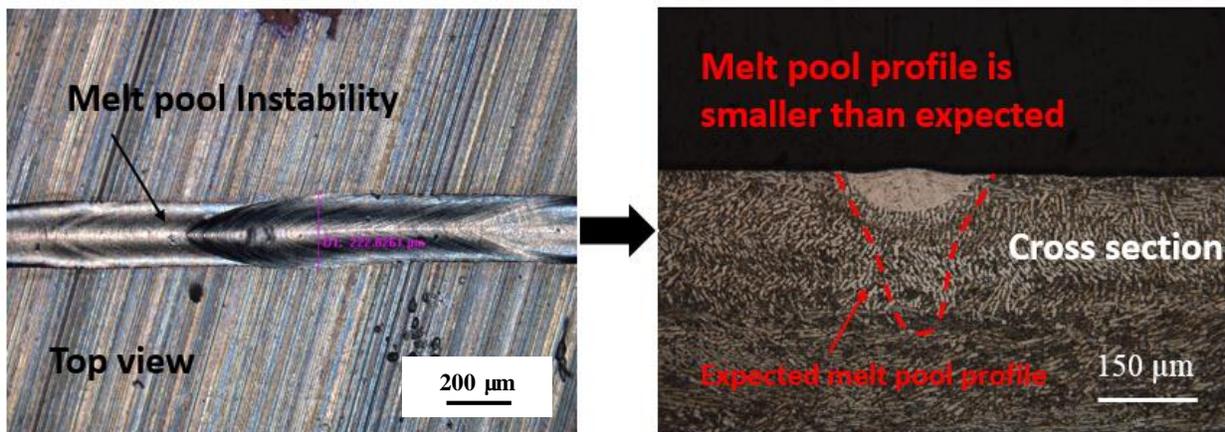
Fig. 8 Unanticipated melt pool geometry (195W & 400mm/s)

For the powder case, Ti-6Al-4V powder and base plate were melted and fused together to form a melt pool, as shown in Fig. 9. These melt pools also solidified into α' phase, similar to the no powder case. When powder is present, the emboss height is a little higher than that of the no powder case. But for melt pools significantly deeper than the powder layer thickness, there is little difference between the geometrical characteristics of the powder case and the no powder case. This means that, besides melting powder, most of the radiation energy is converted to thermal energy to form a melt pool, and then conducted downwards to the base plate.
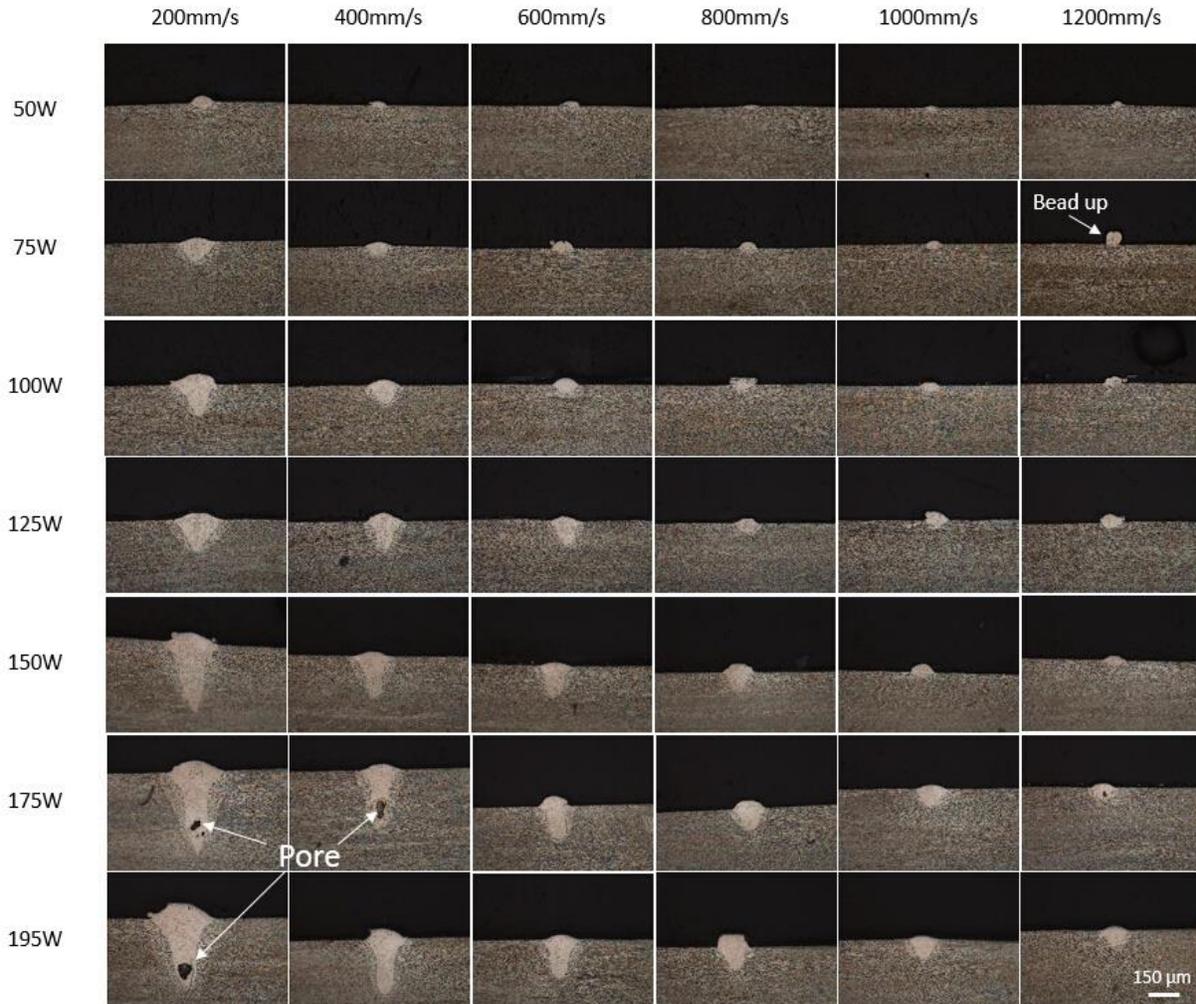
Fig. 9 Melt pool profile of single beads (powder case)

When the energy density is at a high level, one layer of powder (30 μm) does not significantly influence the shape of the melt pool. This porosity becomes entrapped in SLM parts and results in defects. These defects form within deep melt pools which have a characteristic "keyhole" shape with a wider upper head and relatively sharp point at the base, as shown in Fig. 10. These geometrical features are different from the simulated shapes predicted by most heat transfer models for SLM [6]. Another effect of process parameters which result in keyhole geometry is that the large penetration depth may cause additional melting-solidification history in already processed materials, and a larger heat affected zone, causing a more complicated phase transition history for Ti-6Al-4V. The mutual influence of defects and α' phase may result in quality

issues for as-built SLM parts [7]. Therefore, parameter combinations which yield keyhole geometry and porosity are not recommended for SLM processes.

Low laser power and fast scan speeds cause a reduction of energy penetration into Ti-6Al-4V powder. The melt pool may form a round cross section above the base plate, which is the "bead up" or "balling" phenomenon [8, 9], as shown in Fig. 10. The balling effect results when molten material fails to wet the base plate and surface tension forms a round shape. Thus, these process parameter combinations of low energy density are also not suitable for powder bed fusion processes.
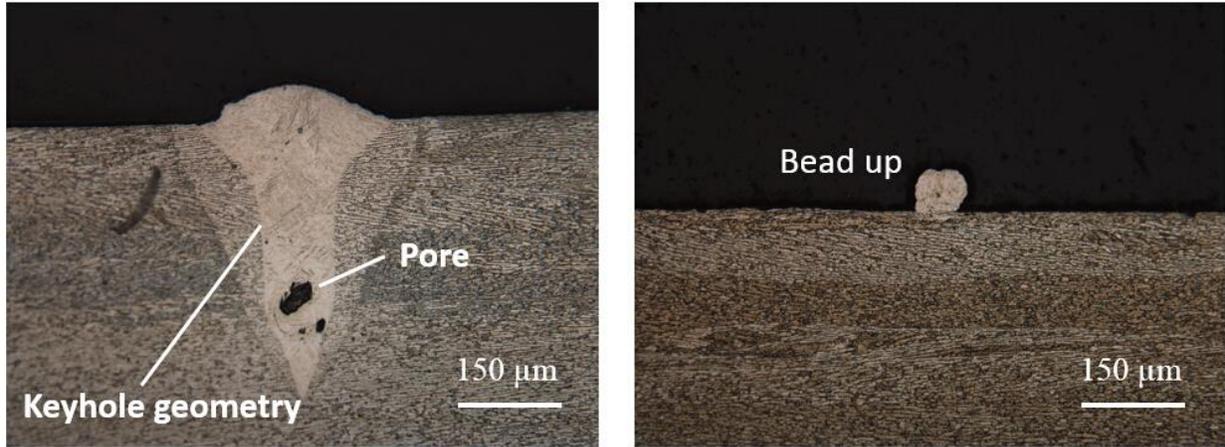
Fig. 10 "Pore" and "bead up" phenomena for the powder case

Fig. 11 shows the melt pool widths measured according to the cross-sectional geometrical profiles. The dimensions for melt pool width measured from cross-sections are comparable to the single bead widths measured from surface measurements, with similar trends for the various laser power and scan speed combinations shown in Fig. 6. Hatch spacing distance can be determined as a fraction of melt pool dimensions, in particular the width of single beads or melt pools. Each hatch spacing distance value thus corresponds to a laser power and scan speed combination, and test pads can be fabricated using these hatch spacings.
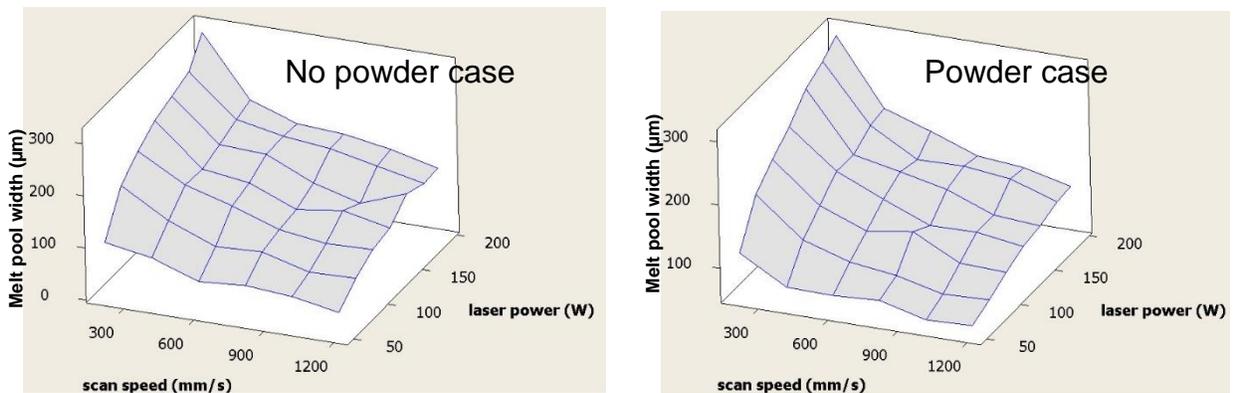
Fig. 11 3D visualization of melt pool width

Test pad experiment

It was found that single bead width and melt pool width are approximately linearly distributed when the scan speed is fixed. A regression curve can be used to predict the width of the melt pool (or single bead) for any laser power. A linear variation of melt pool width is considered a universal regularity in this study. Therefore, instead of directly applying the experimental melt pool widths, the widths are deduced according to the regression equations. Hatch spacing distance is generated by applying a factor to every deduced melt pool width. The standard parameters for an EOS DMLS system for Ti-6Al-4V powder are taken as a reference to determine the numerical relationship between hatch spacing and melt pool width. Based on the experimental melt pool width and hatch spacing distance (from EOS system default parameters), a factor value of 0.74 is applied to the deduced melt pool widths (powder case) to generate the hatch spacing distance for each laser power and scan speed combination. By doing so, overlap between adjacent tracks can be expected for surface continuity.

Multi-layer pads were fabricated using these parameters (laser power, scan speed, and corresponding hatch spacing) at a layer thickness of 30 μm for validation. A raster scan was conducted for each layer, along the *X*-axis or *Y*-axis, as shown in Fig. 12. Without support structure, 33 layers were directly deposited on a base plate to achieve a multi-layer pads with about 1mm thickness. In order to simplify the process, only a hatching scan was carried out for each layer, and no pre- or post-contouring scan was done. As shown in Fig. 12, all pads (totally 42 pads) were successfully fabricated.
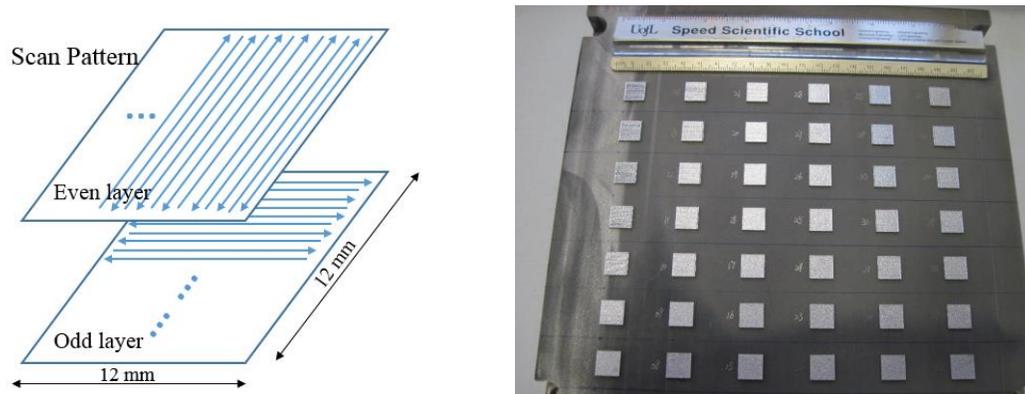
Fig. 12 Scan pattern and multi-layer pads of validation experiment

Slight contact between some pads and the recoating blade took place when recoating the powder, especially for high laser power and low scan speed combinations. It is assumed that over-melting of Ti-6Al-4V powder causes a protruded melt pool shape which resulted in a limited gap between the pads and the blade. The surface topology of multi-layer pads were observed for porosity and quality evaluation, as shown in Fig. 13.

Fig. 13 Top surface topology of multi-layer pads

Although hatch spacing distances were selected with the consideration of overlapping between scan tracks, not all the top surfaces of multi-layer pads show an acceptable morphology to ensure a fully dense part. It is noted that numerous pores and/or lack of fusion sites can be observed on some top surfaces, especially for parameter combinations of low energy density. The melt pool discontinuities can be attributed to several possible reasons. Firstly, for some parameter combinations, melt pool depth may be less than the layer thickness. Some un-melted powder particles could be entrapped causing an unstable melt pool, which results in pores between and along scan tracks. Secondly, a uniform hatch spacing factor (0.74 in this study) may not be suitable for all parameter combinations. As illustrated in Fig. 9, the melt pools show different profiles at various parameters. Therefore, it is better to simultaneously take into account the geometrical and dimensional characteristics of melt pool for selecting a proper factor value. Thirdly, the melt pool shape on the base plate may not exactly represent the actual melt pool morphology on a multi-layer pad. The mutual effects of scan tracks and sequential layers cause a more complicated heat transfer process when compared to single beads on the base plate. The melt pool is more easily influenced when the energy density is low, because the melt pool size is comparable to the average particle size.

265

As for the process parameters of high laser power and low scan speed, clear scan tracks can be observed on the top surface. Hatch spacing distance ensures appropriate overlap between scan tracks. However, as mentioned in the previous section, porosity may be included inside SLM parts. Therefore, these process parameters which yield keyhole geometry and porosity should not be used for the SLM process.

Based on the surface topology, some parameter combinations with medium energy density could be used or further investigated for optimized parameters of SLM Ti-6Al-4V powder. For example, parameters where laser power is larger than 150W, while scan speed is larger than 600 mm/s. The surface morphology of these multi-layer pads shows continuous scan tracks and proper overlap. No apparent pores were observed on the top surface. It is assumed that fully dense parts could be fabricated using the parameters selected within this area, if appropriate hatch spacing distance is selected. Moreover, thermal deformation and deposition efficiency should also be considered for a set of optimized parameters for SLM. Nevertheless, melt pool characterization is able to provide significant information for rapid determination of process parameter ranges for optimization of SLM process parameters.

Conclusions and Future work

The melt pool characteristics, such as geometrical and dimensional features, provide significant information for process parameter selection. Single beads can be easily fabricated and analyzed for melt pool characterization, significantly reducing time and cost compared to conventional optimization methods based on more extensive experimentation. Process parameters, such as hatch spacing, can be down-selected based on a constant multiple or pre-set parameters. In this study, laser power and scan speed were selected from a wide range based on a constant layer thickness. According to the melt pool characterization results, hatch spacing distance can be deduced based on the melt pool or single bead width. This procedure shows flexibility for process parameter selection, and multiple parameter combinations which result in dense parts can be identified quickly. Moreover, only a few simple experiments were needed for obtaining melt pool characteristics. Consequently, efficiency is greatly promoted and the cost of development for new SLM powder is reduced.

The disadvantage of melt pool characterization from single beads on a base plate is that the melt pool may not be reflective of the morphology of the melt pool when built away from the base plate within the powder bed, or on top of a porous support structure. Therefore, more accurate information from single beads or pads generated on support structures is needed. Moreover, incorporation of modeling and simulation into this rapid optimization method may provide more efficient and predictable results for the SLM process.

Acknowledgements

References

[1] I. Gibson, D. Rosen, B. Stucker, Additive manufacturing technologies: rapid prototyping to direct digital manufacturing, Springer, New York, 2009.

[2] L. Li (2006). Repair of directionally solidified superalloy GTD-111 by laser-engineered net shaping. Journal of Materials Science, 41, 7886-7893.

[3] A. Squillace, U. Prisco, S. Ciliberto, A. Astarita (2012). Effect of welding parameters on morphology and mechanical properties of Ti-6Al-4V laser beam welded butt joints. Journal of Materials Processing Technology, 212, 427-436.

[4] R. Rai, J. W. Elmer, T. A. Palmer, T. DebRoy (2007). Heat transfer and fluid flow during keyhole mode laser welding of tantalum, Ti-6Al-4V, 304L stainless steel and vanadium. Journal of Physics D: Applied Physics, 40, 5753-5766.

[5] S. Pang, W. Chen, W. Wang (2014). A quantitative model of keyhole instability induced porosity in laser welding of titanium alloy. Metallurgical and Materials Transactions A: Physical Metallurgy and Materials Science, 45, 2808-2818.

[6] A. V. Gusarov, I. Yadroitsev, Ph. Bertrand, I. Smurov (2009). Model of radiation and heat transfer in laser-powder interaction zone at selective laser melting. J. Heat Transfer, 131(7), 072101 (10 pages).

[7] H. Gong, K. Rafi, T. Starr, B. Stucker (2012). Effect of defects on fatigue tests of as-built Ti-6Al-4V parts fabricated by selective laser melting. Solid Freeform Fabrication Symposium, Austin Texas 2012, 499-506.

[8] N. K. Tolochko, S. E. Mozzharov, I. A. Yadroitsev, T. Laoui, L. Froyen, V. I. Titov, M.B. Ignatiev (2004). Balling processes during selective laser treatment of powders. Rapid Prototyping Journal, 10, 78-87.

[9] J. P. Kruth, L. Froyen, J. Van Vaerenbergh, P. Mercelis, M. Rombouts, B. Lauwers (2004). Selective laser melting of iron-based powder. Journal of Materials Processing Technology, 149, 616-622.